

# Zinc oxide nanoparticles from microwave-assisted solvothermal process: Photocatalytic performance and use for wood protection against xylophagous fungus

Matheus Lemos de Peres<sup>1</sup>, Rafael de Avila Delucis<sup>1</sup>, Sandro Campos Amico<sup>2</sup>, and Darci Alberto Gatto<sup>1</sup>

## Abstract

Nano- and micro-oxides are promising materials due to several interesting characteristics such as photocatalytic and antimicrobial role. In this work, zinc oxide nanorods were obtained by microwave-assisted solvothermal process and their photocatalytic performance and action for wood protection against wood-decay fungus was studied. The morphological (scanning electron microscopy and transmission electron microscopy analyses), microstructural (X-ray powder diffraction analysis) and chemical (infrared spectroscopy) characteristics of the oxide-based nanostructures were investigated. Moreover, photocatalytic performance was evaluated using methylene blue and methyl orange. The nanostructured zinc oxide was impregnated to pinewood samples at 1–5% content and tested for decay resistance using a white-rot fungus. Zinc oxide nanorods agglomerated as urchin-like structures presented high crystallinity, high purity, and high photocatalytic activity. Zinc oxide impregnation was effective in improving pinewood decay resistance, yielding similar protection compared to traditional wood preservative.

## Keywords

ZnO-wood composite, antimicrobial, photocatalyst, biodegradation, microwave-assisted synthesis

Date received: 27 July 2019; accepted: 22 August 2019

Topic: Polymer Nanocomposites and Nanostructured Materials

Topic Editor: Leander Tapfer

Associate Editor: Leander Tapfer

## Introduction

A photocatalytic process consists of several chemical events wherein an electron–hole  $h^+$  is used for oxidizing and, sometimes, capturing electrons for a reduction process, leading to the formation of superoxide anions and hydrogen peroxide ( $H_2O_2$ ) from oxygen.<sup>1</sup> According to Serrano et al.,<sup>1</sup> a heterogeneous photocatalytic process starts when a photon reaches the photocatalyst surface with an amount of energy equal to or greater than its band gap (BG), leading to the formation of mobile electrons in the conduction band (CB) and positive holes in the valence band (VB).

Studies on the photocatalytic performance of some metal oxides have been conducted since the 1970s. More recently, micro- and nanoceramics have been designed to act as absorbents of ultraviolet (UV) radiation, which may

<sup>1</sup> PPGCEM, Federal University of Pelotas, Pelotas/RS, Brazil

<sup>2</sup> PPGCEM, Federal University of Rio Grande do Sul, Porto Alegre/RS, Brazil

### Corresponding author:

Rafael de Avila Delucis, PPGCEM, Federal University of Pelotas, R. Benjamin Constant, 989, Pelotas/RS 96010-610, Brazil.

Email: r.delucis@hotmail.com



be of interest for applications such as photovoltaic cells for direct conversion of solar energy into storable electrical energy, sensing devices, air and water purifiers and coatings of organic substrates to prevent weathering.<sup>2,3</sup>

Ceramic particles such as titanium dioxide (TiO<sub>2</sub>) have also been incorporated into wood to increase its mechanical, hygroscopic and antimicrobial properties,<sup>4</sup> being an alternative for traditional wood preservatives based on waterborne salts, for example, copper-based formulations such as chromium, copper, arsenic and chromium, copper, boron (CCB). These products are effective but remain in the wood for several years after the end of their useful life, bringing environmental issues related to their disposal.<sup>4,5</sup>

A promising substitute for TiO<sub>2</sub> is zinc oxide (ZnO), which has wide BG of 3.37 eV and similar photocatalytic capacity,<sup>6</sup> although it presents higher photocorrosion susceptibility when illuminated by UV rays.<sup>7</sup> Its morphology, especially the position of BG potentials and recombination of charge carriers generated by UV irradiation, limits its absorption capacity to wavelengths below 387 nm.<sup>8</sup>

Adekele et al.<sup>9</sup> described the photocatalytic reaction mechanism of ZnO particles in the presence of methylene blue (MB) as adsorption of MB on ZnO particles; electrons (e<sup>-</sup>) in the VB of dye-sensitized ZnO are excited to the CB under UV light, with simultaneous production of holes (h<sup>+</sup>) in the VB; the dissolved oxygen (O<sub>2</sub>) in aqueous solution acts as electron scavenger and reacts with e<sup>-</sup> to yield active free radicals; the separated holes react with e<sup>-</sup> donors yielding active free radicals; and finally, surface-adsorbed MB molecules are attacked by the generated holes and other free radicals, leading to discoloration and opening-reactions.

The antimicrobial mechanism of ZnO has been described as ZnO forms free electrons from its CB and positively charged emissions in the VB when subjected to a light source; their vacancies reduce the O<sub>2</sub> from water yielding free radicals and anions; and these products oxidize lipids present in bacteria and fungi membranes and may break their DNA strand and also oxidize nucleotides (responsible for the production of nucleic acids), amino acids and proteins from catalytic centres, leading to the loss of genetic content and consequently hindering the reproductive process.<sup>10</sup>

There are several methods for the production of micro- and nanoparticles from ZnO, including sol-gel, pulsed laser deposition, chemical vapour deposition, electrodeposition, spray pyrolysis, microwave irradiation and hydrothermal synthesis.<sup>11</sup> The use of microwaves allows shorter cycles, lower reaction temperatures and homogenous heat transfer. The solvothermal method leads to the absorption of microwave radiation (2.45 GHz frequency and wavelength operation range of 12.25 cm) and conversion to heat, which increases nucleation rate of the crystal formation.<sup>12</sup>

Regarding solvothermal methods, there is a number of recently published studies that confirm the importance of optimizing the process parameters for each possible

solvent, since particles and nanoparticles with different chemical and morphological characteristics require in-depth studies to assess new technological applications for ZnO. For instance, Golic et al.<sup>13</sup> synthesized, via solvothermal reactions, ZnO from ethanolic zinc acetate solutions in the presence of lithium hydroxide. The powder consisted of a large number of small hexagonal particles, single-crystal rods, some single-crystal plates and irregular-shaped particles. They also reported that the planar structure of the precursor molecule played a major role in the growth of the structures in a slightly acid solution.

Mao et al.<sup>14</sup> produced ZnO micro/nanostructures with different morphologies through a solvothermal process in the presence of surfactants. The as-synthesized ZnO samples comprised nanospheres, hexagonal disks, hexagonal bilayer disc-like structures and three-dimensional (3D) flower-like hierarchitectures due to the surfactant effect. High photocatalytic efficiency was achieved and attributed to the formation of hierarchical structures with good crystallinity, which led to the efficient separation of photogenerated electrons and holes.

Zhu et al.<sup>15</sup> described the production and properties of ZnO rod-assembled microspheres prepared by the microwave-assisted hydrothermal method. Their ZnO powder consisted of nanorods with the diameter of 300 nm and the length of 1 μm. They also reported that the improved catalytic activity may be attributed to structural difference, including morphology, surface orientation and surface defects.

Salah et al.<sup>11</sup> described the production of size-controlled ZnO nanostructures by a microwave-assisted route. They obtained a powder that consisted of 25-nm spherical nanoparticles and micro-sized hexagonal nanorods, which were evaluated as an antimicrobial agent against Gram-negative (*Escherichia coli*), Gram-positive (*Bacillus subtilis*) bacteria and yeast (*Saccharomyces cerevisiae*). Their results showed significant inhibition of the bacterial growth even at low ZnO concentrations.

Since both photocatalytic and antimicrobial effects of these particles are relatively well explained in the literature, their use for wood protection against xylophagous agents seems plausible. Thus, in the present work, ZnO rod-like nanoparticles were produced via microwave-assisted solvothermal (MAS) process and their photocatalytic performance and action for wood protection against wood-decay fungus was studied.

## Materials and methods

### Synthesis and characterization of ZnO nanoparticles

ZnO nanoparticles were produced by the MAS method using a developed formulation rich in organic solvent (i.e. ethanol). For that, 3 mmol of zinc nitrate hexahydrate (purchased by Sigma-Aldrich brand, Unites States) and 60 mmol of sodium hydroxide were solubilized in 5 mL of

deionized water. Then, 1 mmol of polyethylene glycol, molecular weight of  $440 \text{ g mol}^{-1}$ , was solubilized in a mixture of 50 mL of anhydrous ethanol and 10 mL of deionized water. The obtained solution was homogenized in an ultrasonic bath for 10 min. This pre-synthesis was done directly in a polytetrafluoroethylene recipient, which was then placed into a microwave oven (a Panasonic equipment, Japan) at  $140^\circ\text{C}$  for 10 min. The final solution was washed at room temperature with distilled water by centrifugation until complete neutralization ( $\text{pH} = 7$ ) and subsequently dried at  $50 \pm 2^\circ\text{C}$  for 24 h.

The morphological structure of ZnO was assessed by scanning electron microscopy (SEM) analysis, in a JSM 6610LV equipment (JEOL brand, Japan), and transmission electron microscopy (TEM), in a JEM 1400 equipment (JEOL brand, Japan). Mean particle diameter, wurtzite length, rod radius and rod length were determined based on TEM micrographs. For that, the Fiji software, developed by Schindelin et al.,<sup>16</sup> was used to calibrate the pixels from the TEM images.

Degree of crystallinity, particle dimension and related characteristics were analysed using X-ray powder diffraction (XRD) patterns recorded using a D8 Advance diffractometer (Bruker brand, Unites States), with copper  $K_\alpha$  radiation ( $\lambda = 0.15406 \text{ nm}$ ), in the  $5\text{--}120^\circ$   $2\theta$  range, with  $0.025^\circ\text{min}^{-1}$  increments. The chemical structure was evaluated by infrared spectroscopy using an IRPrestige-21 equipment (Shimadzu brand, Japan) on powder samples homogenized with potassium bromide pellets. A total of 64 scans ( $500\text{--}4000 \text{ cm}^{-1}$  range) in direct transmittance were performed at  $4 \text{ cm}^{-1}$  resolution.

### Photocatalytic performance

Two dyes based on MB and methyl orange (MO) were used for evaluating photocatalytic response of ZnO nanoceramics. For that, 100 mL of aqueous solution was prepared with  $1.25 \text{ mg L}^{-1}$  of dye and  $0.002 \text{ g L}^{-1}$  of ZnO nanoparticles. The solution was kept under magnetic stirring and placed into a prismatic black wooden box (internal dimensions:  $50 \times 20 \times 20 \text{ cm}^3$ , height is the larger dimension), where it was subjected to UV radiation from a 9-W compact lamp (Osram brand, Germany), with a wavelength of  $315\text{--}400 \text{ nm}$  (UV-A) and dimensions of  $16.7 \times 1.2 \text{ cm}^2$  (length  $\times$  diameter). Aliquots were hourly sampled for 8 h and analysed by UV-VIS spectroscopy in an SP 1105 equipment (Bel Photonics brand, Italy). Two parameters related to dye degradation were calculated, namely  $\ln C_0/C$  and rate constant ( $k$ ), as described in the literature.<sup>9</sup> The former represents the concentration of aqueous solution in the dye, and the latter is the linear fitting coefficient for single dyes and dyes with ZnO particles.

### Wood treatment and decay tests

Three healthy pine trees were randomly selected in a homogenous forest located at Southern Brazil following ASTM

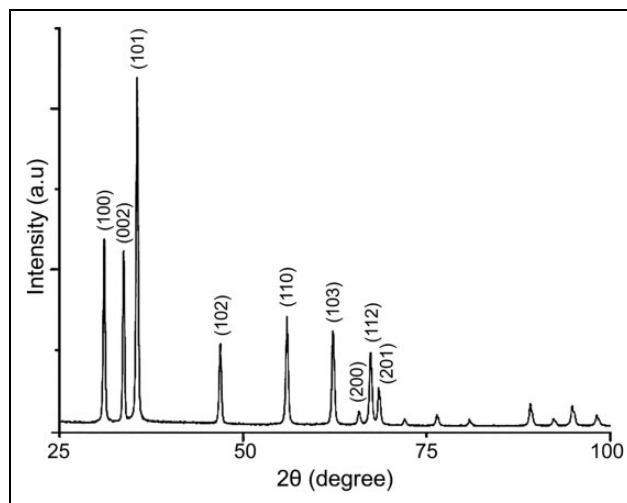


**Figure 1.** XRD pattern of the produced ZnO nanoparticles. XRD: X-ray powder diffraction; ZnO: zinc oxide.

D5536. From each felled tree, a 2.0-m long baseline log was obtained at a height of 10 cm from the ground. From the logs, 8-cm-thick central planks were obtained and then subjected to outdoor drying for about 3 months. After that, prismatic wood samples were cut with the following dimensions:  $2.5 \times 2.5 \times 0.9 \text{ cm}^3$  (length  $\times$  width  $\times$  thickness). The ZnO powders were mechanically homogenized in distilled water:ethanol (1:1) solution at three concentrations, 1%, 2.5% and 5%. This solution was placed in a desiccator under an initial vacuum of 600–700 mmHg for 30 min and then impregnated into the wood samples under constant pressure of 8 bar for 1.5 h, following a modified Bethell process. A final vacuum of 600–700 mmHg was applied for 15 min to remove non-impregnated substances.

The lab test of resistance to fungal decay was carried out based on modified ASTM D2017. Sabouraud agar was inoculated with a white-rot fungus (*Ganoderma applanatum*) into Petri dishes (120 mm diameter). Pristine wood and wood samples treated with ZnO particles were evaluated and compared to samples treated by CCB impregnation as the positive control group. For that, 1 L of 3% aqueous solution of CCB (63.5% of potassium dichromate, 26% of copper sulphate and 10.5% of boric acid) was prepared according to ABNT NBR 9480. The decay tests were performed at  $23 \pm 2^\circ\text{C}$  and relative humidity (RH) of  $60 \pm 5\%$  for an incubation period of 16 weeks inside a laminar flow hood. The wood samples were then conditioned in a climatic chamber at  $23 \pm 2^\circ\text{C}$  and RH of  $50 \pm 5\%$  until constant mass. Mass loss due to fungal attack was calculated based on the initial dry mass.

Rockwell hardness was acquired on the transverse plane of the wood with a benchtop durometer (Digimess brand) for pristine and decayed samples. A one-fourth-inch spherical penetrator was used and 10 Newtons (N) preload was applied. Hardness data were statistically analysed using

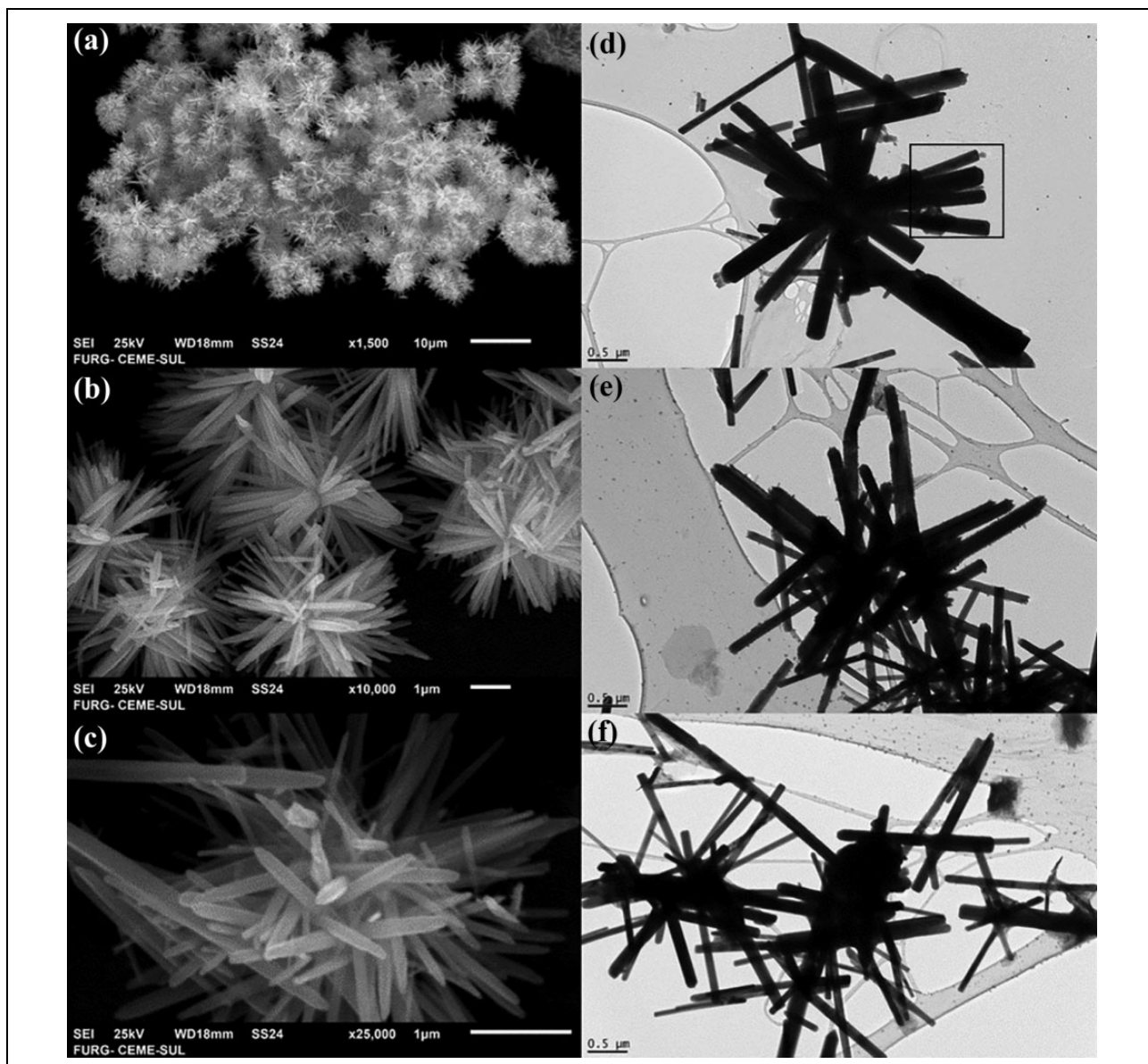


**Figure 2.** SEM (a) to (c) and TEM (d) to (f) images of the produced nanorods agglomerated as urchin-like structures. SEM: scanning electron microscopy; TEM: transmission electron microscopy.

one-way analysis of variance test, followed by mean tests according to Tukey method.

Chemical changes in wood due to the decay exposition were evaluated by infrared spectroscopy using the same procedure and equipment mentioned above. The infrared spectra were mathematically modified to present the differences between reads before and after the decay, as suggested in the literature.<sup>17</sup>

## Results and discussion

### Structure and morphology

Figure 1 shows the X-ray diffractograms, wherein all main peaks are attributed to hexagonal wurtzite structures, in

agreement with the Inorganic Crystal Structure Database Card (ICSD card no. 57450). This hexagonal form for ZnO has lattice constants of  $a = 0.3249$  nm and  $c = 0.5206$  nm (JCPDS, no. 36-1451), and this indicates that the prepared sample is pure ZnO of high crystallinity and free from impurity phases.<sup>7,15</sup> Moreover, an average crystallite size of 154.5 nm was determined in accordance with previous studies.<sup>18</sup> Nevertheless, it is important to mention that distinct particle shapes and dimensions could be obtained using other synthesis methods (e.g. sol-gel),<sup>7,18</sup> based on other equations or calculations after SEM analysis<sup>14</sup> and dynamic light scattering (DLS) measurements.<sup>19</sup>

Figure 2(a) to (f) shows SEM and TEM images of the produced nanorods. The MAS process originated nanorods

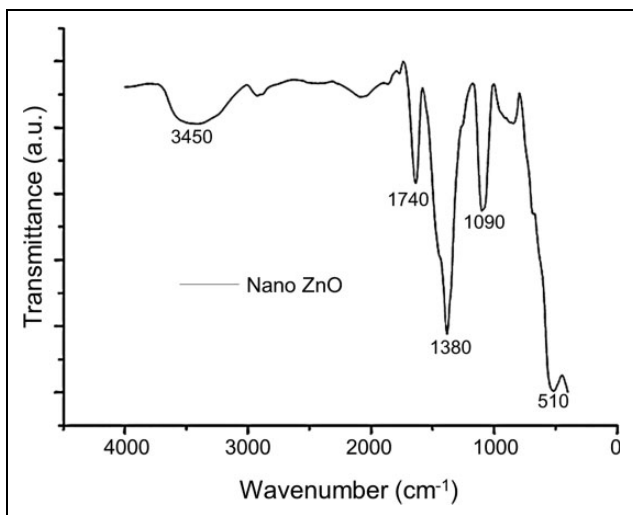


**Figure 3.** Infrared spectra of the ZnO nanoparticles. ZnO: zinc oxide.

or needle-like particles with the largest dimension along the *c*-axis, and mean dimensions of  $0.167 \pm 0.05 \mu\text{m} \times 1.63 \pm 0.33 \mu\text{m}$  (diameter  $\times$  length) based on 60 measurements performed in the square are shown in Figure 2(d). This particle diameter average (approximately  $0.167 \mu\text{m}$ ) is similar to that crystallite size measured by XRD diffraction (approximately  $0.154 \mu\text{m}$ ), which indicates that the ZnO nanorods may be single crystals. Therefore, it is also important to consider that Scherrer's formula is not applicable for long particles like the ZnO nanorods of the present study, which presented 1630 nm in average length (*c*-axis, along the (001) direction), determined by SEM.

Those SEM and TEM micrographs indicate that these rods have attached ends, that is, urchin-like structures, which are the typical hexagonal wurtzite structure of ZnO crystalline.<sup>15,20</sup> When incorporated into ceramic composites, however, these particles can resemble nanospheres,<sup>14</sup> hexagonal disks,<sup>14</sup> hexagonal bilayer disc-like structures,<sup>14</sup> 3D flower-like hierarchitectures<sup>14</sup> or pine cones,<sup>3</sup> which may depend on the initial solution pH.<sup>19</sup> Other studies, such as Benhebal et al.,<sup>7</sup> used the sol-gel method and obtained uniform spherical particles (around  $0.5 \mu\text{m}$  diameter) agglomerated as lamellar clusters.

Qualitative chemical analyses by infrared spectroscopy indicate the presence of typical peaks of ZnO (Figure 3), such as those at 510 and  $1090 \text{ cm}^{-1}$  related to metal oxide stretching vibrations of Zn–O bonds.<sup>21</sup> The peaks at 1380 and  $1740 \text{ cm}^{-1}$  represent stretching vibrations of C=O bonds, and a broad band at  $3450 \text{ cm}^{-1}$  represents stretching vibrations of O–H bonds, which can indicate the presence of impurities and moisture, respectively.<sup>9,21,22</sup> The peak at  $1740 \text{ cm}^{-1}$  can also be related to an additional common band attributed to the bending mode of absorbed water.<sup>23</sup> Moreover, in their study, Pholnak et al.<sup>24</sup> used the same precursor and reported its spectrum with prominent peaks

at 840, 1090 and  $1380 \text{ cm}^{-1}$ , which were attributed to various vibration modes of its nitrate groups.<sup>25</sup>

### Photocatalytic performance

Figure 4(a) and (b) shows UV-VIS spectra of the two dyes used to study the photocatalytic response of the ZnO particles. The spectra show broad absorptions within 550–700 nm and 350–520 nm, with peaks at 660 and 450 nm for MB and MO, respectively. MO also presented two humps at 400 and 500 nm, while MB displayed a single hump at 620 nm. Similar results have been reported for ZnO particles and some doped ceramics.<sup>9,11,26</sup> The absorbance peaks gradually decreased as the irradiation time increased, which confirm dye degradation in some of its chromogenic groups.

$\ln(C_0/C)$  data for single dyes and dyes with ZnO particles displayed linear correlation with irradiation time, as shown in Figure 4(c), similar to literature results.<sup>15</sup> Compared to neat dyes, higher  $R^2$  and  $k$  values (Figure 4(d)) were obtained for the dyes in the presence of the nanoceramics, indicating a photocatalytic effect related to the ZnO. The parameter  $k$  is mainly dependent on particle morphology (i.e. dimension and shape),<sup>15</sup> which varies with the type of precursor, the heating time and the microwave power.<sup>11</sup> For Adekele et al.,<sup>9</sup> a high photocatalytic performance is related to particles with the presence of more reactive ions (species), larger surface area and increased acting sites.

### Decay resistance of ZnO-wood nanocomposites

All ZnO treatments led to improved biological resistance compared to the pristine wood samples (Table 1). Moreover, incorporation of 2.5% or 5% of ZnO particles led to wood protection levels comparable to that of the treatment with CCB (positive control), which confirms the potential application of ZnO particles as wood preservative. Although the ZnO antimicrobial mechanism is not yet fully understood, its antimicrobial performance is well correlated with the degree of crystallinity, particle dimension and amount of  $\text{H}_2\text{O}_2$  generated at the surface of ZnO crystals and can be estimated based on its lattice constant.<sup>11</sup> Similar improvements in wood biological resistance were found for woods treated with  $\text{TiO}_2$ .<sup>4,5</sup>

Table 1 also presents hardness results for pristine and treated woods after the decay tests. The statistical analysis of the mass loss ( $F = 320.17$ ;  $p < 0.01$ ) and hardness ( $F = 8.66$ ;  $p < 0.01$ ) values, treatments with 2.5% and 5% of ZnO particles led to significant protection of the pinewood against fungal attack and contributed to make the surface stiffer, perhaps modifying their viscoelastic behaviour. Also, the ZnO-wood nanocomposites reached similar hardness levels among them.

However, the ZnO treatments were not able to achieve greater protection compared to the CCB

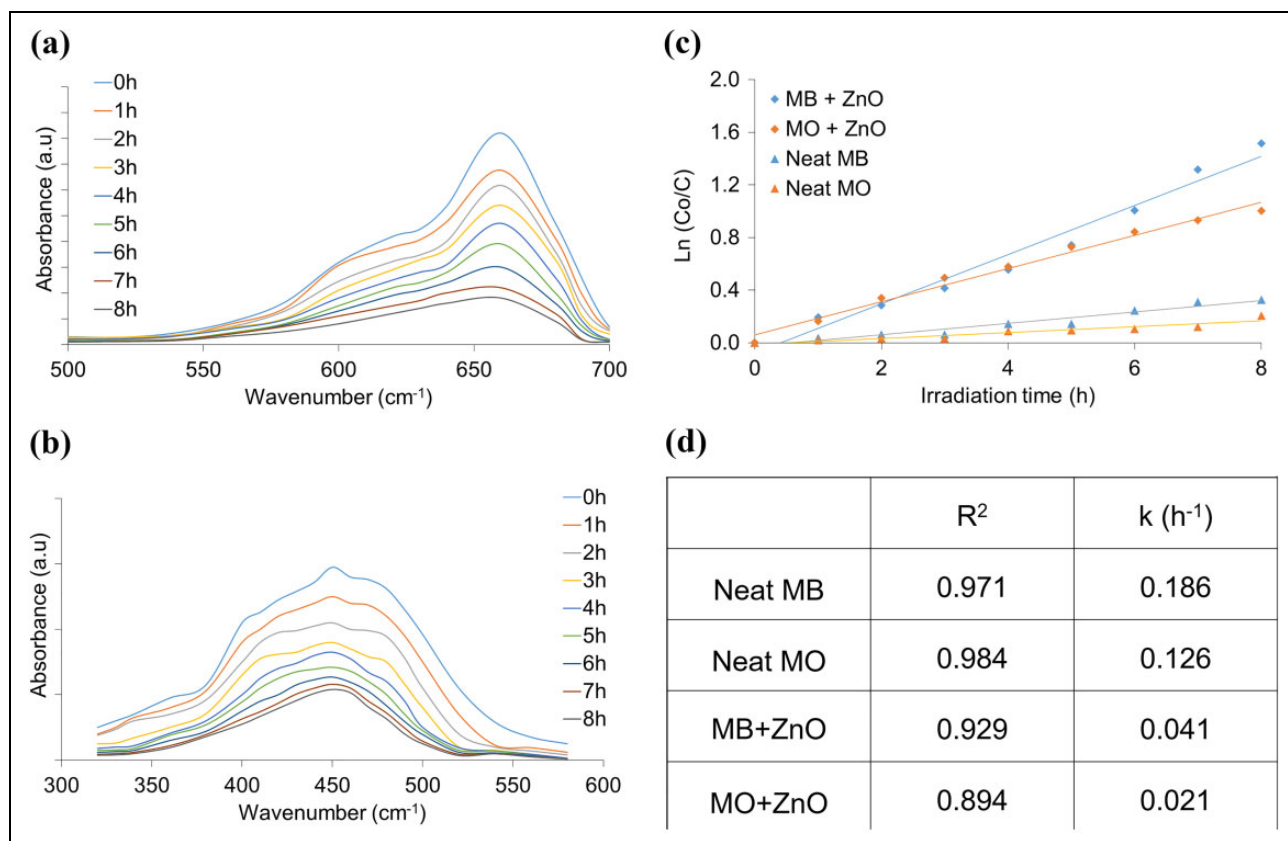


**Figure 4.** Absorbance spectra of MB (a) and MO (b) dye solutions, linear fitting of the  $\ln(C_0/C) \times \text{Time}$  data for both dyes and dyes with nanopowder (c) and photocatalytic performance (d). MB: methylene blue; MO: methyl orange; ZnO: zinc oxide.

**Table 1.** Mass loss, decay ratings (by ASTM D2017) and hardness for pristine and treated woods.

Groups	Mass loss (%) <sup>a</sup>	Decay ratings	Hardness (kgf) <sup>a</sup>
Pristine	26.06 ± 1.95 <b>D</b>	Moderately resistant	14.83 ± 2.44 <b>A</b>
CCB	5.91 ± 1.03 <b>A</b>	Highly resistant	26.50 ± 4.26 <b>B</b>
ZnO 1%	10.96 ± 1.33 <b>C</b>	Resistant	20.66 ± 0.47 <b>AB</b>
ZnO 2.5%	9.22 ± 0.46 <b>BC</b>	Highly resistant	26.00 ± 2.16 <b>B</b>
ZnO 5%	8.63 ± 0.23 <b>B</b>	Highly resistant	25.00 ± 1.02 <b>B</b>

ZnO: zinc oxide; CCB: chromium, copper, boron; kgf: kilogram-force.  
<sup>a</sup>Means with the same letters do not present statistical difference at 95% of confidence level according to Tukey test.

treatment, and the mass loss results were in fact inferior. Even so, pristine and CCB-treated wood samples presented slightly larger deviations, perhaps due to a not fully known effect associated to surface roughness. In wood, the surface quality is dependent on anatomical features, moisture content, machinability and so on, but the effect of each mentioned factor may distinctively affect wood roughness and hardness.

As shown in Figure 5, several peaks commonly related to wood biodegradation were identified in Fourier transform infrared spectra, especially those related to

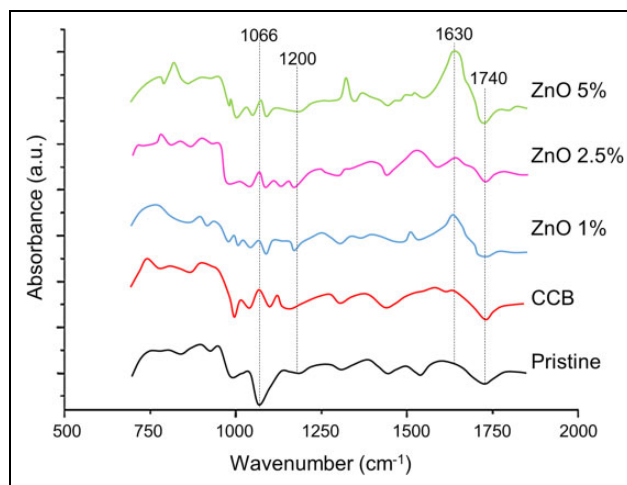


**Figure 5.** FTIR spectra of the differences between exposed and unexposed wood samples. FTIR: Fourier transform infrared; ZnO: zinc oxide; CCB: chromium, copper, boron.

hemicelluloses, including prominent peaks at 1200 and 1740  $\text{cm}^{-1}$ , representing unconjugated C=O stretching in xylan and C=O bond of the carboxylic group, respectively.<sup>27</sup> No peaks related to CCB impregnation were identified.

The pristine wood sample presented a valley at  $1066\text{ cm}^{-1}$ , whereas the other samples presented a prominent peak at this wave number. According to Gallio et al.,<sup>27</sup> this peak may represent C–H deformation in guaiacyl units belonging to lignin that are strongly impacted by white-rot fungi. This also indicates stronger biodegradation rate in pristine wood compared to treated woods, ratifying previous mass loss and hardness results. A prominent peak at  $1630\text{ cm}^{-1}$  for the ZnO-wood nanocomposites is also related to low degradation rates, since it is associated to C=O stretching vibrations in peptide bonds (Amide I) as a result of fungi colonization.<sup>28</sup> Moreover, this peak at  $1630\text{ cm}^{-1}$  can also be attributed to a bending mode of absorbed water.<sup>29</sup>

## Conclusions

ZnO nanorods agglomerated as urchin-like structures have been successfully synthesized by the MAS method. The ZnO presented high crystallinity, high purity and high photocatalytic activity for decolorization of MB and MO solutions under UV light.

The ZnO impregnation was effective in improving the pinewood decay resistance against white-rot fungi, especially above 2.5% content, hindering the access of the fungus to the lignin proteins, as confirmed by infrared spectroscopy and mass loss results. The wood protection induced by ZnO nanoparticles was similar to that of traditional CCB impregnation, as confirmed by hardness results, which confirms the potential of ZnO particles to be used as wood preservative. These results suggest that pinewood treated via impregnation of ZnO nanoparticles can be used for indoor applications. Further studies may include leaching tests after ZnO impregnation into wood to ascertain the potential of this nanocomposite for outdoor use.

## Acknowledgements

The authors would like to thank CAPES for supporting this work.


## Declaration of conflicting interests

The author(s) declared no potential conflicts of interest with respect to the research, authorship, and/or publication of this article.

## Funding

The author(s) received no financial support for the research, authorship, and/or publication of this article.

## ORCID iDs

Rafael de Avila Delucis  <https://orcid.org/0000-0002-3657-9216>

Sandro Campos Amico  <https://orcid.org/0000-0003-4873-2238>

## References

1. Serrano B, Salaices M, Ortiz A, et al. Quasi-equilibrium and non-equilibrium adsorption in heterogeneous photocatalysis. *Chem Eng Sci* 2007; 62(18–20): 5160–5166.
2. Kumar A, Gupta A, Sharma KV, et al. Use of aluminum oxide nanoparticles in wood composites to enhance the heat transfer during hot-pressing. *Eur J Wood Wood Prod* 2013; 71(2): 193–198.
3. Jiang H, Zhang X, Gu W, et al. Synthesis of ZnO particles with multi-layer and biomorphic porous microstructures and ZnO/rGO composites and their applications for photocatalysis. *Chem Phys Lett* 2018; 711: 100–106.
4. Zanatta P, Lazarotto M, Cademartori PHG, et al. The effect of titanium dioxide nanoparticles obtained by microwave-assisted hydrothermal method on the color and decay resistance of pinewood. *Maderas-CiencTecnol* 2017; 19(4): 495–506.
5. Marzbani P, Afrouzi YM and Omidvar A. The effect of nano-zinc oxide on particleboard decay resistance. *Maderas-Cienc Tecnol* 2015; 17(1): 63–68.
6. Roy N, Chowdhury A and Roy A. Observation of negative differential resistance and electrical bi-stability in chemically synthesized ZnO nanorods. *J Appl Phys* 2014; 115: 223502–223508.
7. Benhebal H, Chaib M, Salmon T, et al. Photocatalytic degradation of phenol and benzoic acid using zinc oxide powders prepared by the sol-gel process. *Alexandria Eng J* 2013; 52(3): 517–523.
8. He Y, Wang Y, Zhang L, et al. High-efficiency conversion of CO<sub>2</sub> to fuel over ZnO/g-C<sub>3</sub>N<sub>4</sub> photocatalyst. *Appl Catal B Environ* 2015; 168–169: 1–8.
9. Adekele JT, Theivasanthi T, Thiruppathi M, et al. Photocatalytic degradation of methylene blue by ZnO/NiFe<sub>2</sub>O<sub>4</sub> nanoparticles. *Appl Surf Sci* 2018; 455(15): 195–200.
10. Sirelkhatim A, Mahmud S, Seeni A, et al. Review on zinc oxide nanoparticles: antibacterial activity and toxicity mechanism. *Nano-Micro Lett* 2015; 7(3): 219–242.
11. Salah N, Al-Shawafi W, Alshahrie A, et al. Size controlled, antimicrobial ZnO nanostructures produced by the microwave assisted route. *Mater Sci Eng C* 2019; 99: 1164–1173.
12. Bilecka I and Niederberger M. Microwave chemistry for inorganic nanomaterials synthesis. *Nanoscale* 2010; 2(8): 1358–1374.
13. Golic DL, Branković Z, Daneu N, et al. Solvothermal syntheses of nano- and micro-sized ZnO powders with a controllable morphology. *J Sol-Gel Sci Technol* 2012; 63(1): 116–125.
14. Mao Y, Li Y, Zou Y, et al. Solvothermal synthesis and photocatalytic properties of ZnO micro/nanostructures. *Ceram Int* 2019; 45(2): 1724–1729.
15. Zhu Z, Yang D and Liu H. Microwave-assisted hydrothermal synthesis of ZnO rod-assembled microspheres and their photocatalytic performances. *Adv Powder Technol* 2011; 22(4): 493–497.
16. Schindelin J, Arganda-Carreras I, Frise E, et al. Fiji: an open-source platform for biological-image analysis. *Nat Methods* 2012; 9(7): 676–682.
17. Preklet E, Tolvaj L, Bejo L, et al. Temperature dependence of wood photodegradation. Part 2: evaluation by Arrhenius law. *J Photochem Photobiol A Chem* 2018; 356(1): 329–333.

18. Xiao S, Liu L and Lian J. Solvothermal synthesis of nanocrystalline ZnO with excellent photocatalytic performance. *J Mater Sci Mater Electron* 2014; 25(12): 5518–5523.
19. Chakrabarti S and Dutta BK. Photocatalytic degradation of model textile dyes in wastewater using ZnO as semiconductor catalyst. *J Hazard Mater* 2004; 112(3): 269–278.
20. Samat NA and Nor RM. Sol–gel synthesis of zinc oxide nanoparticles using *Citrus aurantifolia* extracts. *Ceram Int* 2013; 39(1): 545–548.
21. Trindade LG, Minervino GB, Trench AB, et al. Influence of ionic liquid on the photoelectrochemical properties of ZnO particles. *Ceram Int* 2018; 44(9): 10393–10401.
22. Asgharian M, Mehdipourghazi M, Khoshandam B, et al. Photocatalytic degradation of methylene blue with synthesized rGO/ZnO/Cu. *Chem Phys Lett* 2019; 719(16): 1–7.
23. Maheswari CM, Reddy KO, Dhlamini MS, et al. Extraction and structural characterization of cellulose from milkweed floss. *Separ Sci Technol* 2017; 52(17): 2677–2683.
24. Pholnak C, Sirisathitkul C, Suwanboon S, et al. Effects of precursor concentration and reaction time on sonochemically synthesized ZnO nanoparticles. *Mater Res* 2014; 17(2): 405–411.
25. Li P, Xu ZP, Hampton MA, et al. Control preparation of zinc hydroxide nitrate nanocrystals and examination of the chemical and structural stability. *J Phys Chem C* 2012; 116(18): 10325–10332.
26. Tahir K, Ahmad A, Li B, et al. Visible light photo catalytic inactivation of bacteria and photo degradation of methylene blue with Ag/TiO<sub>2</sub> nanocomposite prepared by a novel method. *J Photochem Photobiol B Biol* 2016; 162: 189–198.
27. Gallio E, Zanatta P, Ribes D, et al. Fourier transform infrared spectroscopy in treated woods deteriorated by a white rot fungus. *Maderas-Cienc Tecnol* 2018; 20(3): 479–488.
28. Wang X, Chen X, Qi Z, et al. A study of *Ganoderma lucidum* spores by FTIR microspectroscopy. *Spectrochim Acta A Mol Biomol Spectrosc* 2012; 91: 285–289.
29. Reddy OK, Maheswari CU, Dhlamini MS, et al. Extraction and characterization of cellulose single fibers from native African Napier grass. *Carbohydr Polym* 2018; 188: 85–91.